



Green synthesis of SnO₂ nanoparticles using *Delonix elata* leaf extract: Evaluation of its structural, optical, morphological and photocatalytic properties

K. C. Suresh¹ · S. Surendhiran² · P. Manoj Kumar² · E. Ranjith Kumar³ · Y. A. Syed Khadar⁴ · A. Balamurugan⁵ 

Received: 11 June 2020 / Accepted: 16 September 2020 / Published online: 25 September 2020
© Springer Nature Switzerland AG 2020

Abstract

This research article reports the green synthesis of SnO₂ nanoparticles and its structural, optical, morphological and photocatalytic behaviors has been achieved by using *Delonix elata* leaf extract. Three different synthesis routes (i.e., sonication, wet chemical, and microwave method) are employed to prepare SnO₂ nanoparticles. A comparative analysis was performed on the main physical properties to get a broader understanding of the effect of processing parameters on prepared SnO₂ nanoparticles. The prepared SnO₂ nanoparticles were characterized using different techniques like TG, XRD, FESEM, EDX, FT-IR, UV-Vis, PSD, and BET surface area analysis. Furthermore, the application of the prepared SnO₂ nanoparticles as photocatalyst was proceeded to degrade rhodamine B dye.

Keywords Green synthesis · SnO₂ NPs · *Delonix elata* leaf extract · Photocatalytic applications

1 Introduction

In the Present-day society, industrial wastewater with an extreme level of organic dyes has raised with the ratio of industrial development. These organic dyes from the outlet of various manufacturing sectors such as plastic, textile, and leather, food, pharmaceutical, and chemical are hazardous to humans [1]. Apart from various diseases and disorders caused by this high toxic of organic dyes, it also severely affect the ecosystem and cause dangerous pollutions (i.e.,) groundwater contamination [1]. The photosynthetic process was limited in the aquatic plants by blocking sunlight, and the oxygen capacity of water was reduced for the normal growth of marine animals due to the high toxicity of organic dyes [2]. Removal of dangerous dyes and toxic organic compounds from wastewaters,

photocatalysts process is the most commonly employed techniques [3]. In the past few decades, enormous effects have been taken for health risk assessment on dangerous dyes and against pollutants to reduce groundwater contamination. Wide range of photocatalysts employing nano metal oxides like titanium dioxide (TiO₂), zinc oxide (ZnO), tin oxide (SnO₂), cadmium sulfide (CdS) and etc., [4–7]. It has proved its properties in degrading a heterogeneous of distinct organic dyes and other pollutants of water into degradable compounds. Amid the dissimilar types of photoactive catalysts, nano metal oxides have been usually premeditated for this reason [8–10]. Various dopants are also used to enhance the dye degradation properties of the aforementioned nano photocatalyst [11–13]. One of the best nano photocatalysts in nano metal oxides with an excellent n-type semiconductor having bandgap energy

✉ Y. A. Syed Khadar, dryaskh@gmail.com; ✉ A. Balamurugan, bala.snr@gmail.com | ¹Department of Physics, Research and Development Centre, Bharathiar University, Coimbatore, Tamilnadu 641 046, India. ²Centre for Nanoscience and Technology, KS Rangasamy College of Technology, Tiruchengode, Tamilnadu 637 215, India. ³Department of Physics, KPR Institute of Engineering and Technology, Coimbatore, Tamilnadu 641 407, India. ⁴Department of Physics, KS Rangasamy Arts and Science College for Women, Tiruchengode, Tamilnadu 637 215, India. ⁵Department of Physics, Government Arts and Science College, Avinashi, Tamilnadu 641 654, India.



of 3.6 eV was tin oxide (SnO₂) nanoparticles [14]. Tetragonal crystal configuration of SnO₂ nanoparticles has latent applications in the pitch of catalysis, rechargeable lithium batteries, optoelectronic devices, and transparent conducting electrodes [15–18].

Different methods have been worn for the synthesis of SnO₂ nanoparticles, such as sol–gel [19], hydrothermal [20], co-precipitation [21], Microwave-assisted methods [22], spray pyrolysis [23]. But the green synthesis of nanoparticles has more attention compared with the aforementioned methods. The main reason behind the green approach for the preparation of nano metal oxides is getting hold of additional importance such as cost-effective, high yield nanoparticle production, etc., compared with other methods [24, 25]. There are limited papers reported studies of green synthesis of SnO₂ using plant extracts as capping and reducing agents towards photocatalytic applications.

The *Delonix elata* (*D. elata*) tree belongs to *Caesalpinioideae* family. The flowering timbers are the genus members. It has been explored for many pharmaceutical applications as the leaves and bark of this plant is known to have medicinal properties [26]. It is found all over south India. *D. elata* leaf extract contains unique phenolic compounds mainly two flavanones namely Quercetin and Rutin [27]. Table 1 summarizes the compound details which were identified from *D. elata* leaf extract.

In this present study, the authors report the most economical and easiest green synthesizes protocol to prepare SnO₂ nanoparticles using *D. elata* leaf extract as a chelating agent. The three different methods i.e., wet chemical, sonication, and microwave methods were influenced to prepare SnO₂ nanoparticles. The motive for taking these three different processing methods is

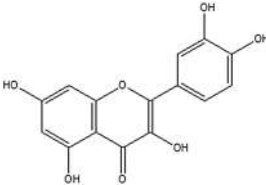
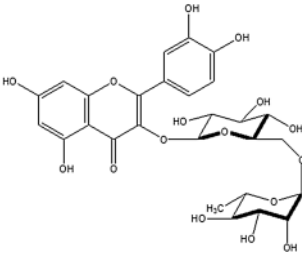
due to its simplicity and also simply a scalable attribute. Along with it, all three processes reveal an excellent ability of conserve the chemical precursor i.e., bulk production of nanoparticles can be achieved from the very small amount of the starting precursor. Even though the processes seemed quite similar yet they are extremely different in terms of its processing parameters and play a dominant role in particle size, purity, and crystalline nature, morphology, specific surface area of nanomaterials [28]. The influences of these preparation methods on structural, morphological, optical, and photocatalytic properties of SnO₂ nanoparticles were comprehensively discussed. The prepared SnO₂ nanoparticles were proceeding for Rhodamine B (RhB dye) degradation under UV light irradiation.

2 Materials and methods

2.1 Preparation of *D. elata* leaf extract

The *D. elata* leaves were collected from villages in Namakkal district, Tamil Nadu, India. The collected leaves were washed with deionized water (DI) to remove the moisture present on it. After washing, the leaves were allowed to dry at room temperature for two days. The dried leaves were powdered by using a domestic mixer (mixie) and then the 10 g of the powdered leaf was dispersed in 300 mL of DI water and soaked in Erlenmeyer flask. The dispersion was heated at 70 °C for 30 min. The leaf extract is been allowed to cool to room temperature without disturbances, and filtered with the help of Whatmann No. 1 filter paper. The final filtrate was stored for further experimental use.

Table 1 Chemical compounds from the extract of *D. elata* leaf (Adapted from Ref. [27])

S. No	Name of the compounds	Structure of the compound	Molecular formula
1	Quercetin		C ₁₅ H ₁₀ O ₇
2	Rutin		C ₂₇ H ₃₀ O ₁₆

2.2 Synthesis of SnO₂ nanoparticles

The SnO₂ nanoparticles were green synthesized using the leaf extract of *D. elata* through three different synthesis routes namely i.e., Sonication, wet-chemical, and microwave methods. The base solution was prepared by adding 2.256 g of tin chloride (0.1 M) precursor, (an analytical grade (AR) from Merck, India) to 100 ml of *D. elata* leaf extract and stirred for 24 h at constant rpm to synthesize SnO₂ nanoparticles. Hereafter this solution is called as a base solution for the preparation of SnO₂ nanoparticles. All the AR grade chemicals were utilized without any further purification. The synthesis parameters for the aforementioned synthesis routes were employed to a base solution. The synthesis protocol for SnO₂ nanoparticles using *D. elata* leaf extract is shown in Fig. 1.

2.2.1 Wet-chemical method

For synthesizing SnO₂ nanoparticles through the wet-chemical route, the base solution was agitated vigorously using a magnetic pellet under elevated temperature (70 °C) for 1 h, and then the precipitate was formed. Then, the base solution was dried at 100 °C for 12 h, followed by centrifuge at 5000 rpm, washed several times with DD water, and ethanol, finally, obtained products was calcined at 400 °C for 2 h. The calcined powder i.e., SnO₂ nanoparticles was used for further characterization. Now the procured SnO₂ nanoparticles were termed as SnO₂-WC nanoparticles.

2.2.2 Sonication method

The sonication process at 40 kHz (Advanced Sonicator, Lark, New Delhi, India) was employed over the prepared base solution for 1 h, till a clear suspension was obtained. Following the suspension of the precipitates in the base

solution, it was dried in a hot air oven at 100 °C for 12 h. The dried precipitate was collected and centrifuged at 5000 rpm, washed several times with double distilled water and absolute ethanol, then calcined at 400 °C for 2 h, to produce SnO₂ nanoparticles which were exploited for further characterization studies [29]. The obtained SnO₂ nanoparticles are termed as SnO₂-SO nanoparticles.

2.2.3 Microwave method

In a typical synthesis of the microwave method, the base solution was taken in Teflon lined vessel which was subject to microwave radiation power (320 W) at constant temperature 100 °C for 15 min and then allowed to cool at room temperature. Final yellow-colored products were collected, centrifuged at 5000 rpm, washed multiple times with double distilled water, and absolute ethanol which is kept in an oven at 100 °C for 3 h. The SnO₂ nanoparticles were then obtained by calcinations of as-prepared powder in air at 400 °C for 2 h. The procured SnO₂ nanoparticles are termed as SnO₂-MW nanoparticles.

2.3 Characterisation techniques

The X-ray diffraction patterns of the prepared SnO₂ nanoparticles were obtained by using a powder X-ray diffractometer (XRD; X'Pert PRO, PANalytical, Almelo, the Netherlands) operated with the Cu at 40 kV and 30 mA. The XRD pattern was analyzed in the 2θ range from 20 to 80°. The Fourier transforms infrared (FTIR) spectra of the SnO₂ nanoparticles were recorded using an FTIR spectrophotometer (Spectrum 100; PerkinElmer, USA) in the range of 4000–450 cm⁻¹ using KBr as an active medium by mixing 200:1 ratio of KBr. The particle size analyzer (Nanophox Sympatec Germany) used to decide the common particle size distribution primarily based on the dynamic light scattering (DLS) method and laser light of wavelength 633 nm. It was measured in the range from 1 to 1000 nm at a scattering angle of 90°. The measurement was continuously repeated for five-times to get average particle size. The average particle size of SnO₂ nanoparticles was calculated by using the automated mode. The UV–visible (UV–vis) spectrophotometer (Agilent Cary 8454, Singapore) was used to determine the absorbance capability of the prepared SnO₂ nanoparticles with distilled water as a solvent for a wide range from 180–800 nm wavelength of electromagnetic spectral region. The specific surface area (SBET) was calculated using the Brunauer–Emmett–Teller (BET) process using a BET surface area analyzer (Autosorb AS-1MP; Quantachrome, Boynton Beach, FL). The sample was degassed under vacuum at 363 K for 3 h to remove the physisorbed moisture. The physisorption study was carried out with N₂ adsorption–desorption measurements

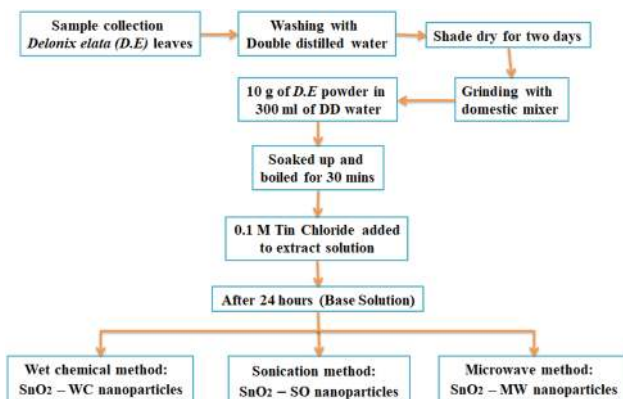


Fig. 1 Synthesis protocol for SnO₂ nanoparticles

under liquid N₂ temperature. The mean pore size distributions and total pore volume were calculated using the Barrett–Joyner–Halenda (BJH) method. The thermal degradation properties of the prepared SnO₂ nanoparticles were evaluated by using Thermogravimetric analyzer and Differential thermal analyzer (Exstar TG/DTA 6300, Hitachi, Tokyo, Japan) with a heating rate of 10 °C/min up to 1000 °C at nitrogen atmosphere.

2.4 Photocatalytic degradation activity

The photocatalytic dye degradation activity of the green synthesized SnO₂ nanoparticles was carried out by assessing the degradation of the RhB dye in an aqueous solution under constant UV light irradiation. In the photocatalytic degradation process, a standard volume of RhB dye was taken and 20 mg of each SnO₂ nanoparticles were added to RhB dye solution [30]. The photoreaction was performed in a cubic UV reaction chamber having an annular UV illumination. Irradiation was provided using a 40 W UV lamp with major emission at 365 nm, located at the corners of the UV reactor (Agilent, Singapore). With the effect from UV light irradiation, for every 30 min once, 5 ml of the aqueous solution was collected from the UV reaction chamber and subjected to measure the UV absorbance range of RhB dye at λ_{max} = 556 nm. The photocatalytic dye degradation efficiency of the prepared SnO₂ nanoparticles was calculated by using the following Eq. (1) [29]

$$\eta = \left[\frac{C_0 - C_t}{C_0} \right] \times 100\% \quad (1)$$

Here, η is the degradation percentage, C_0 is the initial absorbance of dye (at 00 min); C_t is the change in absorbance of the dye at after time intervals of the degradation.

3 Results and discussion

3.1 Fourier transform infrared spectra (FTIR)

3.1.1 FTIR spectra of *D. elata* leaf extract

The FT-IR study of *D. elata* leaf extract is shown in Fig. 2. The functional groups of the organic and functional compounds of the leaf extract were determined. Infrared spectrum shows band area 3420 cm⁻¹ is the presence of O–H groups of leaf extract. The peak area at 2920 cm⁻¹ is related to vibration C–H ring stretching. The band area at 2860 cm⁻¹ shows symmetric C–H stretching. A strong stretching vibration at 1630 cm⁻¹ shows the presence of carbonyl (C=O) groups. The absorption band at

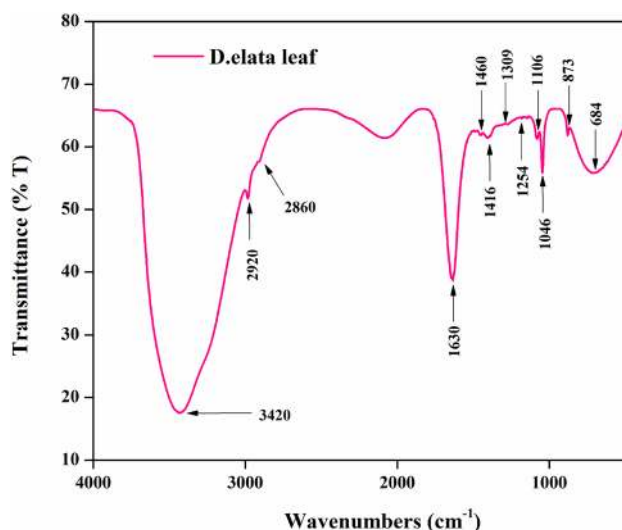


Fig. 2 FTIR spectra of *D. elata* leaf extract

1460 cm⁻¹ corresponds to vibrations of NH plane bending. The band area a 1416 cm⁻¹ shows CH₂ bending.

The peak at 1309 cm⁻¹ indicated by the presence of alkyl ketone components. The band area 1254 cm⁻¹ shows the sulphonic acid esters (SO₃). 1106 cm⁻¹ band area is showing C–O–C aryl conjugated group. The band at 1046 cm⁻¹ shows C–N stretching alkyl amine and peak at 873 cm⁻¹ show the C–H out plane bending. The band areas from 684 to 450 cm⁻¹ shows halogen compounds like C–Cl, C–Br, and C–I compound [31].

The polyhydroxyl compounds namely Quercetin and Rutin existing in the *D. elata* leaf extract act as ligation agents and the aromatic hydroxyl groups of Rutin react readily with tin ions, which lead to the formation of a stable complex of SnO₂ nanoparticles [27]. The complex was decomposed at the calcination process which gave rise to SnO₂ NPs. The possible phytochemical reaction during the synthesis process of SnO₂ nanoparticles using *D. elata* leaf extract is given in Fig. 3 [32].

3.1.2 FTIR spectra of SnO₂ nanoparticles

The FT-IR spectra were shown in Fig. 4a–c respectively for SnO₂–WC, SnO₂–SO, SnO₂–MW nanoparticles. The FTIR spectra of SnO₂ nanoparticles have the major bands at 3434 cm⁻¹, 2920 cm⁻¹, 2848 cm⁻¹, 1618 cm⁻¹, 1381 cm⁻¹, 608 and 506 cm⁻¹ [33]. The broad band around at 3365 to 3620 cm⁻¹ and 1618 cm⁻¹ due to stretching vibrations of Sn–OH groups and due to O–H stretching vibrations of water molecules absorbed from the environment by SnO₂ nanoparticles and which may present in the surface of the SnO₂ nanoparticles [33]. The band area around 2848 and 2920 cm⁻¹ indicates the presence of C–H group. The

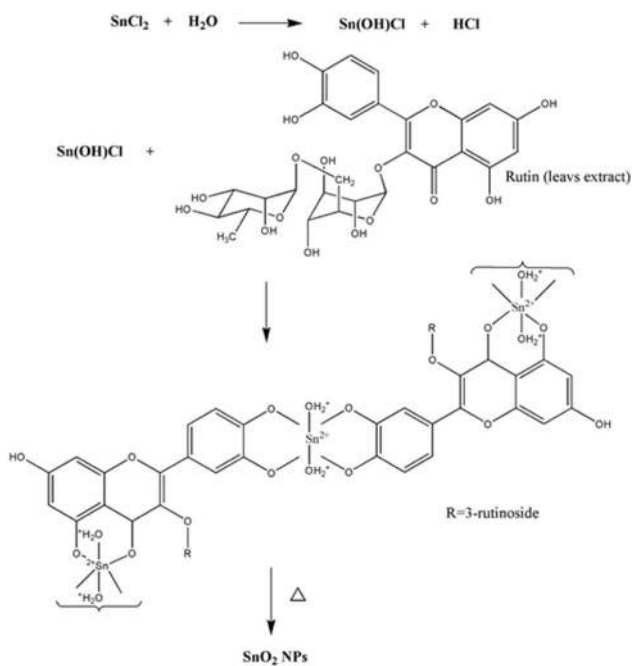


Fig. 3 Formation of SnO₂ nanoparticles

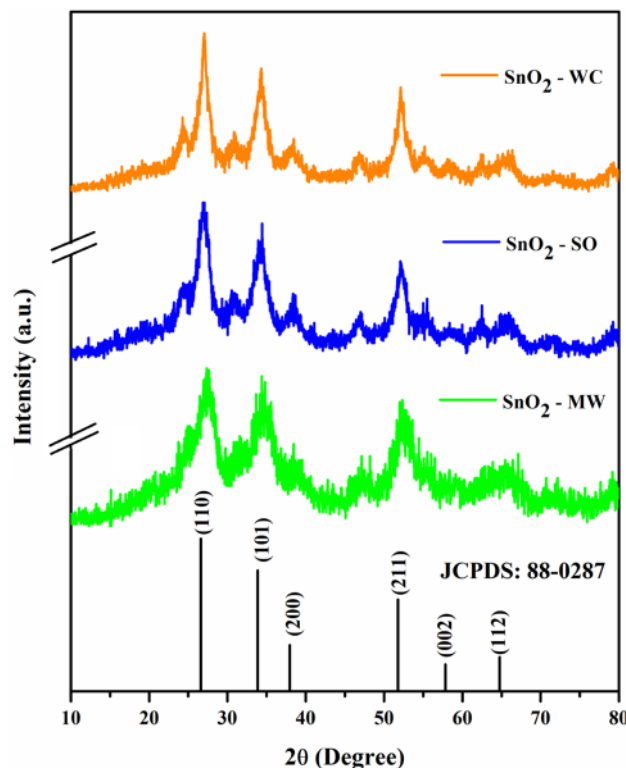


Fig. 5 XRD pattern for SnO₂ nanoparticles

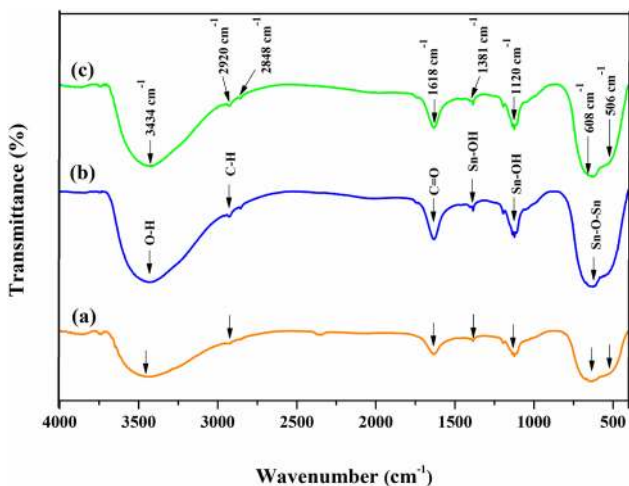


Fig. 4 shows FTIR Spectra of a SnO₂-WC, b SnO₂-SO, and c SnO₂-MW nanoparticles

peak area around 500 to 650 cm⁻¹ is ascribed to the Sn–O stretching vibration and the O–Sn–O bending vibration, respectively. For the above reason, the existence of these bands confirmed the formation of SnO₂ nanoparticles [33, 34].

3.2 X-ray diffraction patterns (XRD)

The XRD patterns of SnO₂ nanoparticles were represented in Fig. 5. The XRD studies confirmed the presence

of high crystalline SnO₂ nanoparticles which was perfectly matched with standard JCPDS No.: 88-0287 for all the SnO₂ nanoparticles but with slight distortion in diffraction angle (2θ) and intensities of the XRD peaks. The diffraction angle values obtained from XRD pattern for SnO₂ nanoparticles are 26.90°, 34.21°, 37.04°, 52.16°, 58.36°, and 65.84°, which are indexed with the (110), (101), (200), (211), (002), (112) planes, respectively. However, it was necessary to note that the intensity of the diffraction peaks shows an increasing trend with a change in synthesis methods. The crystalline SnO₂ nanoparticle formation is high for microwave influenced method compared with the other two methods. The following Debye Scherer Eq. (2) used to determine the crystallite size [35, 36],

$$D = \frac{k\lambda}{\beta \cos\theta} \tag{2}$$

where k is constant (0.9), λ is the wavelength having value 1.540 Å corresponding to Cu Kα source, θ is the Bragg angle and β is the full width of the half maximum.

The calculated crystallite size of SnO₂ nanoparticles was found to be 7.61, 6.09, and 5.92 nm respectively for SnO₂-WC, SnO₂-SO, and SnO₂-MW nanoparticles. The various structural parameters like lattice parameters, unit cell volume, dislocation density and microstrain values of

SnO₂ nanoparticles were calculated by using the following relations and estimated values were tabulated in Table 2.

$$\frac{1}{d^2} = \frac{h^2 + k^2}{a^2} + \frac{l^2}{c^2} \tag{3}$$

$$V = a^2 \cdot c \tag{4}$$

$$\delta = \frac{1}{D^2} \tag{5}$$

$$\varepsilon = \frac{\beta}{4 \tan \theta} \tag{6}$$

3.3 Thermal analysis of SnO₂ nanoparticles

TGA profile curves of the prepared SnO₂ nanoparticles are shown in Fig. 6. Three major weight losses can be observed in the TGA curve at 90 °C (I), 380 °C (II), and 470 °C (III). The minor weight loss (I) in the low-temperature region indicates the presence of a water molecule of the lattice. It is observed that the TGA curve for SnO₂-WC and SnO₂-SO exhibit a weight loss of 25.1 and 24.06% occurred in the temperature range from 300 to 700 K but for SnO₂-MW exhibits 20.51% of weight loss only observed in TGA curve. These results clearly indicate the microwave irradiation makes high thermally stable SnO₂ nanoparticles when compared with the other two methods. Thus the weight losses are due to the water evaporation and decomposition of organic components present in the prepared SnO₂ nanoparticles which may come from *D. elata* leaf extract. Similar weight loss observation of green synthesized SnO₂ nanoparticles are already reported [8].

3.4 Morphological studies of SnO₂ nanoparticles

Figure 7a, c, and e shows the FESEM images of SnO₂-WC, SnO₂-SO, and SnO₂-MW nanoparticles. In Fig. 7a, c, and e shows clusters like foam morphology with small agglomerations for all SnO₂ nanoparticles but SnO₂-MW (Fig. 7e) exhibits the uniform distribution morphology it may be formed due to effects of microwave irradiation during

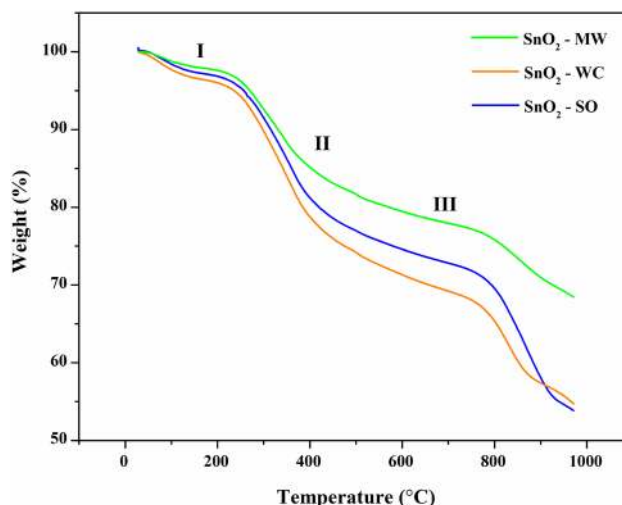


Fig. 6 shows the Thermogravimetric analysis of green synthesized SnO₂ nanoparticles

the synthesis process. The high surface to volume ratio of SnO₂-MW nanoparticles may be due to their uniform distributions and very small-sized cluster like foam morphology in its crystalline and UV absorptions natures [37, 38]. Figure 7b, d, and f shows the EDX spectra of prepared SnO₂ nanoparticles. The EDX spectrum validates that all prepared SnO₂ nanoparticles consist only Sn and O with a very small amount of Cl. The presence of Cl peak in the EDX spectrum may be due to the residue of starting precursor which can be easily removed by undergone through a water wash. Thus, the purity of the prepared SnO₂ nanoparticles is very high. The EDX quantitative results of SnO₂ nanoparticles are given as an inset table in EDX images (Fig. 7b, d, and f).

3.5 Particle size analysis

Figure 8 shows the average particle size distribution of the prepared SnO₂ nanoparticles. The average particle size (d₅₀) of the prepared SnO₂ nanoparticles are found around 13–18 nm. It is in the range of 9.4 (d₁₀)–37.41 (d₉₀), 9.0 (d₁₀)–33.41 (d₉₀), and 6.8 (d₁₀)–27.2 (d₉₀) nm size, respectively, for SnO₂-WC, SnO₂-SO, and SnO₂-MW

Table 2 Structural parameters of SnO₂ nanoparticles obtained from XRD analysis

Sample name	Crystallite size (nm)	Lattice parameter (Å)		Unit cell volume (Å ³)	Dislocation density 'δ' (× 10 ¹⁵ lines/m ²)	Micro strain 'ε' (× 10 ⁻³ /lines·m ⁴)
		a=b	c			
SnO ₂ -WC	7.61	4.659	3.129	67.95	0.1727	6.6871
SnO ₂ -SO	6.09	4.717	3.140	69.89	0.2696	4.6579
SnO ₂ -MW	5.92	4.677	3.202	70.07	0.2853	3.0324
JCPDS No: 88-0287	4.737	3.186	71.51	–	–	–

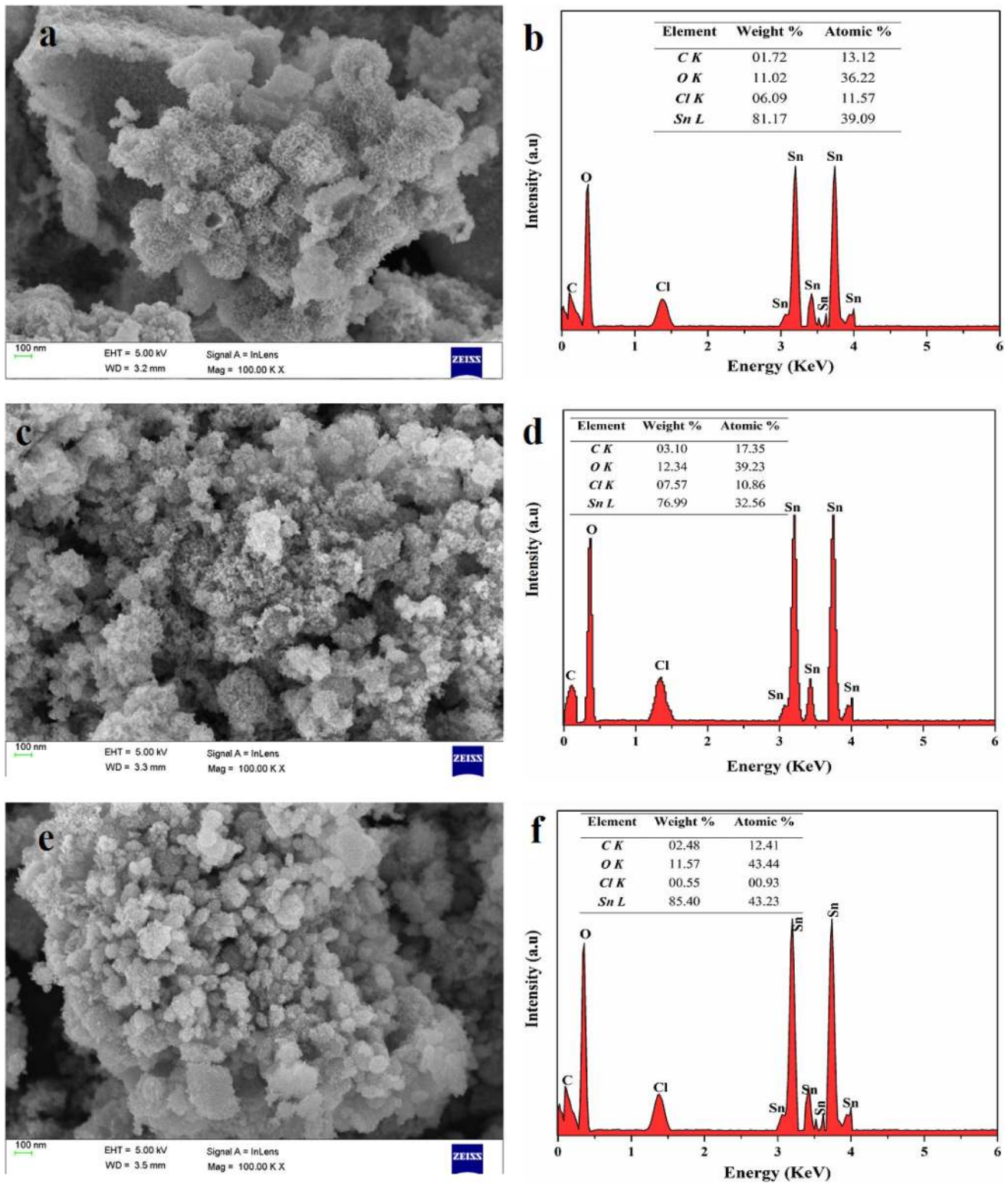


Fig. 7 shows FESEM images (a, c, & d) and EDX pattern of (b, d, & f) SnO₂-WC, SnO₂-SO, and SnO₂-MW nanoparticles

nanoparticles. Moreover, the mean particle size distribution (d_{50}) of SnO₂ nanoparticles is 18.75 ± 3 , 17.40 ± 3 , and 13.68 ± 3 nm, respectively, for samples SnO₂-WC, SnO₂-SO,

SnO₂-MW nanoparticles. It is found that prepared all the SnO₂ nanoparticles influence the formation of particles at nanoscale under different processing methods. The

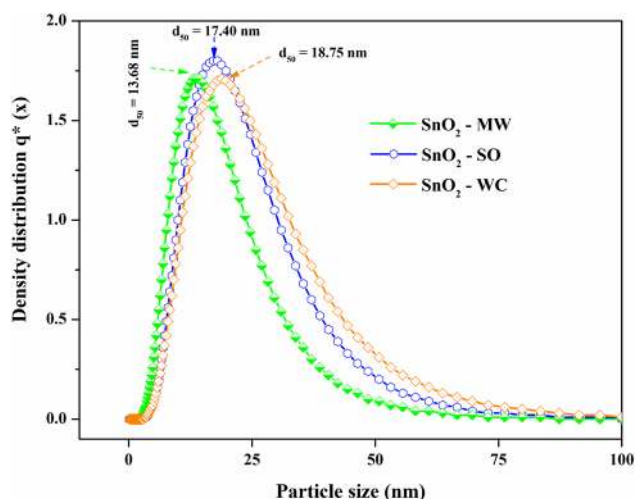


Fig. 8 shows Particle size distribution curve of SnO₂ nanoparticles

SnO₂-MW exhibit a smaller particle size compared to SnO₂-WC and SnO₂-SO, which is also evidenced from the obtained crystalline peaks of XRD.

3.6 Specific surface area analysis

The N₂ adsorption–desorption isotherm of prepared SnO₂ is shown in Fig. 9a and b. The observed BET surface area, pore size, and pore volume of SnO₂ nanoparticles are given in Table 3. The SnO₂ nanoparticles displaced type-IV isotherm from desorption according to the IUPAC nomenclature, but with a major change in the desorption isotherm for all SnO₂ nanoparticles due to particle

Table 3 Nitrogen sorption porosimetry studies and average particle size distributions of SnO₂ nanoparticles

S. No.	Sample	S _{BET}	Pore volume (cm ³ g ⁻¹)	Mean pore size (nm)	Particle size (nm) from DLS
1	SnO ₂ -WC	101	0.5813	15.24	18.75
2	SnO ₂ -SO	169	0.7709	05.29	17.40
3	SnO ₂ -MW	196	1.0081	02.96	13.68

size. In the case of SnO₂-MW and SnO₂-SO, the amount of N₂ adsorption rapidly increases up to a relative pressure of 0.4 beyond which a hysteresis loop is adsorbed in the relative pressure ranges from 0.1 to 0.9. The above observation clearly demonstrated that the existence of mesopores nature as shown in Fig. 9b.

The BET surface area of SnO₂-MW nanoparticles is very high (196 m²g⁻¹) compared with the SnO₂-SO (169 m²g⁻¹), SnO₂-WC (101 m²g⁻¹) nanoparticles. The observed huge BET surface area for the SnO₂-MW is due to its lower particle size (13.68 nm) than SnO₂-SO (17.40 nm), SnO₂-WC (18.75 nm) nanoparticles. It is betrayed from the above observation that the characteristic properties of SnO₂ nanoparticles treated by three different synthesis methods influence the specific surface area i.e., as the average particle size decreases, the specific surface area of the SnO₂ nanoparticle increases. The observed results confirm the relationship between the surface areas to the particle size of the nanomaterials. These investigations denote that the SnO₂ nanoparticles with lower particle size and high surface area may lead to enhance physical and electrical property [39, 40].

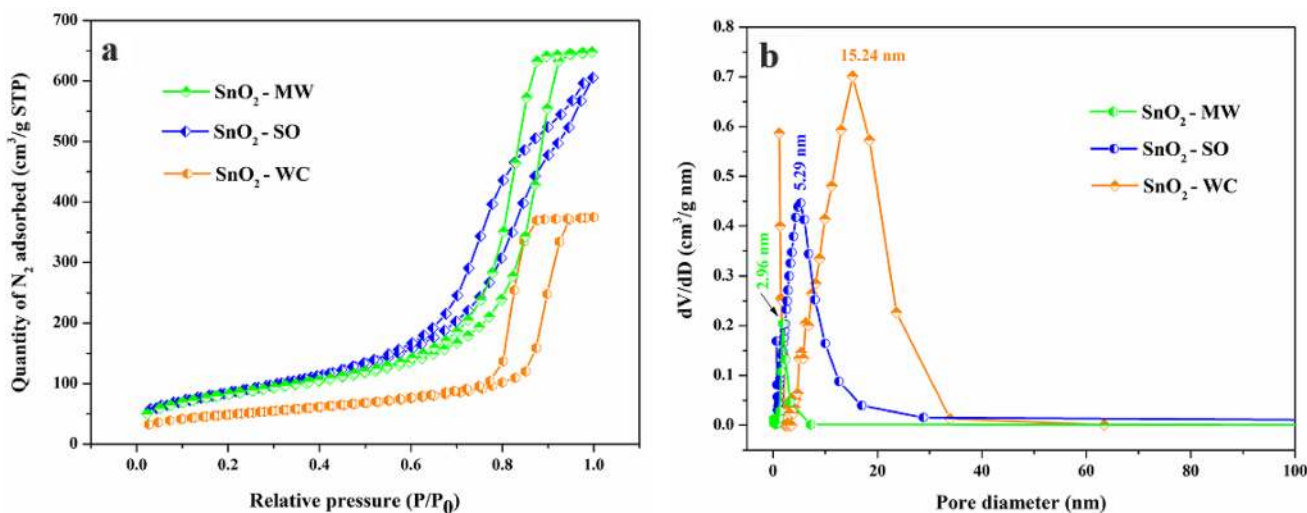


Fig. 9 shows N₂ adsorption – desorption isotherm (a) and BJH pore size distribution curve (b) of SnO₂ nanoparticles

3.7 Optical properties

UV–visible absorption spectra were recorded in order to perceive the optical properties of synthesized SnO₂ nanoparticles. The Fig. 10a represented the UV–vis absorption spectra of SnO₂–WC, SnO₂–SO, and SnO₂–MW nanoparticles. From Fig. 10a it was manifested that broad peaks of infinitesimal intensity commenced beginning around 220 to 260 nm.

It was apparent that the intensity of these broad absorption peaks started to decrease with change in influencing parameters and move towards lower wavelength. The optical properties are strongly depending upon the particle size of the nanoparticles [39, 40]. From the UV–vis spectra, it is evident that the absorption onset shows a blue shift with a decrease in crystallite size. The observed blue shift absorption spectra are the direct consequence of quantum confinement effect which is associated with particle size [35]. Due to the quantum confinement effect, the bandgap of the nanoparticle increases as the particle size decreases and results in the shift of absorption spectra towards a lower wavelength. From the absorption spectra, direct bandgap energy is calculated using Tauc relation which is shown in Fig. 10b. For semiconductor nanoparticles, to relate the absorption coefficient with incident photon energy following equation has been used [4, 35].

$$\alpha(\nu)h\nu = K(h\nu - E_g)^n$$

$\alpha(\nu)$ Absorption coefficient, K is a constant, E_g is energy bandgap, $h\nu$ is incident photon energy, and n equals to ½ for direct bandgap semiconductor and equals to 2 for indirect band gap semiconductors.

The calculated energy bandgap values are 3.80, 3.89, and 3.91 eV respectively for SnO₂–WC, SnO₂–SO, SnO₂–MW nanoparticles.

3.8 Photocatalytic degradation of Rhodamine B dye

The highly possible photocatalytic degradation mechanism of the RhB dye by using prepared SnO₂ nanoparticles can be enlightened by the following standard protocol. When the photocatalyst surface is illuminated with photon energy equals or greater than its natural bandgap energy, it will lead to the formation of holes (h^+) in the valence band and an electron (e^-) in the conduction band of the prepared SnO₂ nanoparticles. The hole (h^+) acts as an oxidizing agent and oxidizes the pollutant directly or water to form hydroxyl radicals of degraded products.

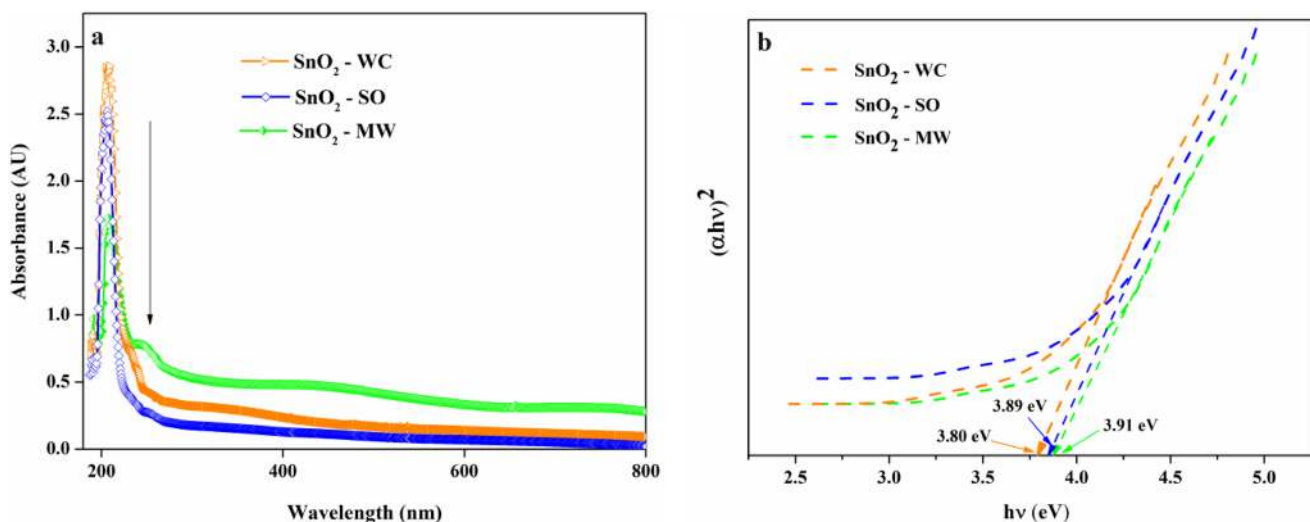
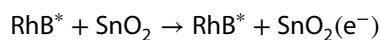
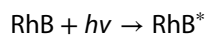
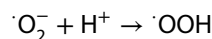
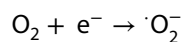
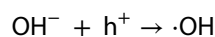
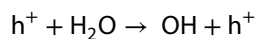
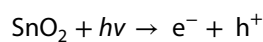


Fig. 10 shows UV–vis absorption spectra and Tauc plot of prepared SnO₂ nanoparticles

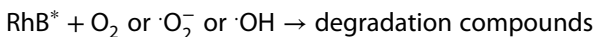
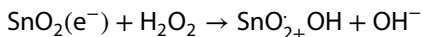
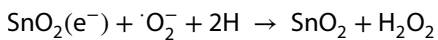
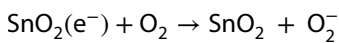


Figure 11a–c shows the photocatalytic degradation process of RhB dye under UV light irradiation for constant time intervals respectively for without SnO₂, SnO₂–WC, SnO₂–SO, SnO₂–MW nanoparticles. After 30 min of UV irradiation, the absorbance peaks of RhB

dye strongly decreased when compared with pure SnO₂ and RhB dye with the addition of SnO₂ nanoparticles.

The results announcing the degradation of RhB dye with the addition of SnO₂ nanoparticles under UV light radiation. The photocatalytic degradation efficiency of SnO₂ nanoparticles was calculated by using Eq. 1. The degradation efficiency of the SnO₂–WC, SnO₂–SO, and SnO₂–MW nanoparticles after 150 min of UV light irradiation are 82.3%, 85.6%, and 92.8% respectively and 5.6% for RhB dye without SnO₂ nanoparticles. The degradation results were clearly indicated that the prepared SnO₂–MW nanoparticle exhibits the improved degradation efficiency compared with SnO₂–WC, and SnO₂–SO nanoparticles.

Its crystalline nature with high in purity, uniformly distributed clusters like foam morphology with higher surface area helps to exhibit better degradation results while

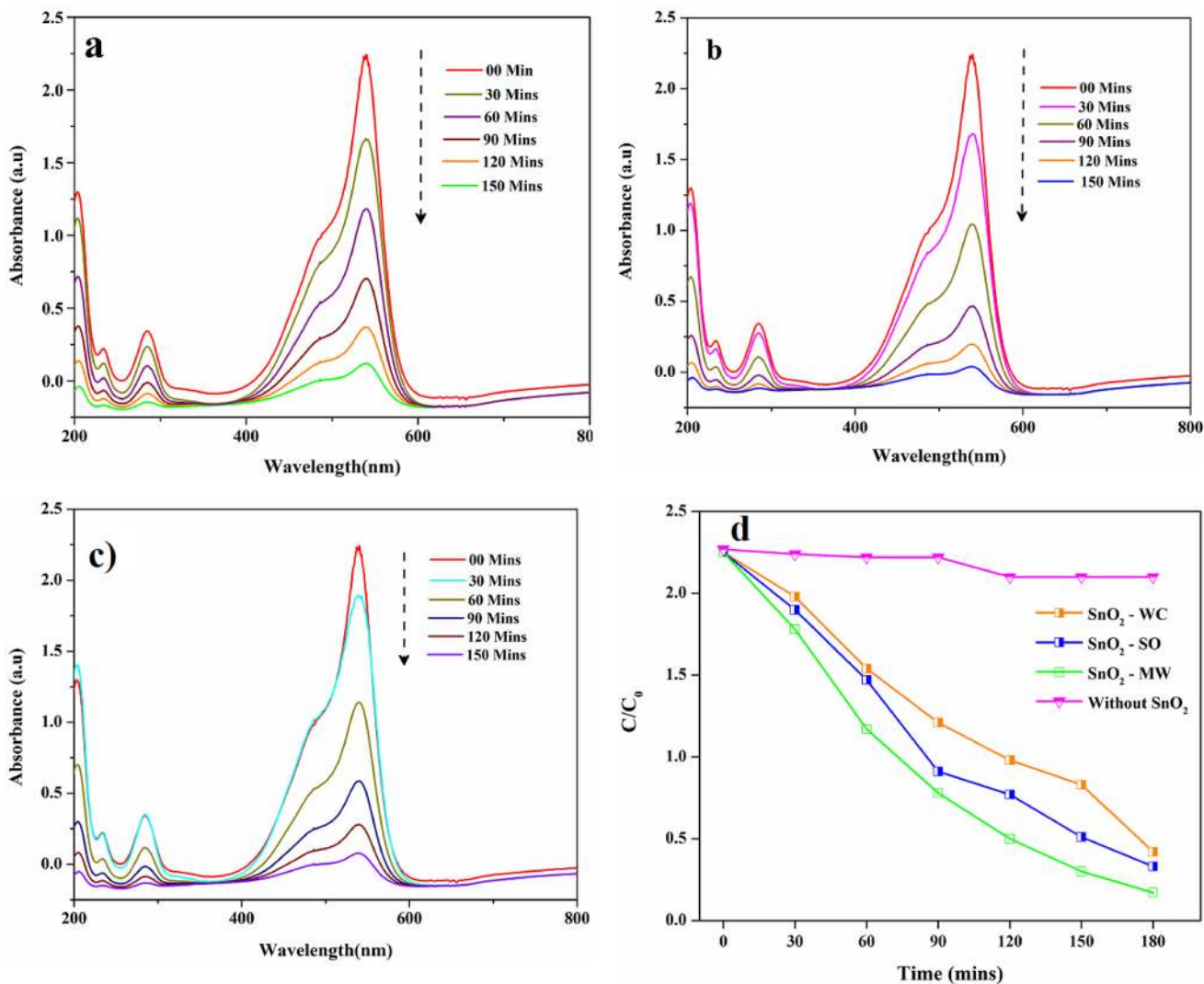


Fig. 11 depicts Photocatalytic responses of **a** SnO₂–WC, **b** SnO₂–SO, **c** SnO₂–MW nanoparticles and **d** degradation efficiency under UV light irradiation

compared with earlier reports [42]. The obtained photocatalytic degradation performances of the prepared SnO₂ nanoparticles were compared with previously published articles which are summarized in Table 4.

After the completion of the degradation process, to confirm the presence of degraded products from RhB dye which were absorbed on the surface of SnO₂ nanoparticles, the photocatalyst was separated from the dye mixture and dried in a hot air oven at 80° C without washing it, and analyzed by FT-IR spectra. The FTIR spectra of SnO₂ nanoparticles after the photocatalytic reaction is shown in Fig. 12. After the degradation process, the intensity of some peaks is reduced and also a few new peaks have been raised while comparing with SnO₂ nanoparticles before the photocatalytic reaction process. These changes are due to the adsorption of degraded compounds from the RhB dye settled on the surface of SnO₂ nanoparticles [41].

4 Conclusion

The highly crystalline SnO₂ nanoparticles were synthesized by novel and eco-friendly routes by employing *D. elata* leaf extract as a reducing agent by influencing three different processes namely wet chemical, sonication, and microwave irradiation. The microwave irradiation influenced SnO₂ nanoparticles shows (SnO₂-MW) excellent crystallinity and nanoparticles exhibit higher surface area 196 m²g⁻¹ compared with the other two methods. Due to the influencing process, particle sizes of the prepared SnO₂ nanoparticles are gradually decreased. The microwave irradiated SnO₂ nanoparticles show the excellent photocatalytic degradation

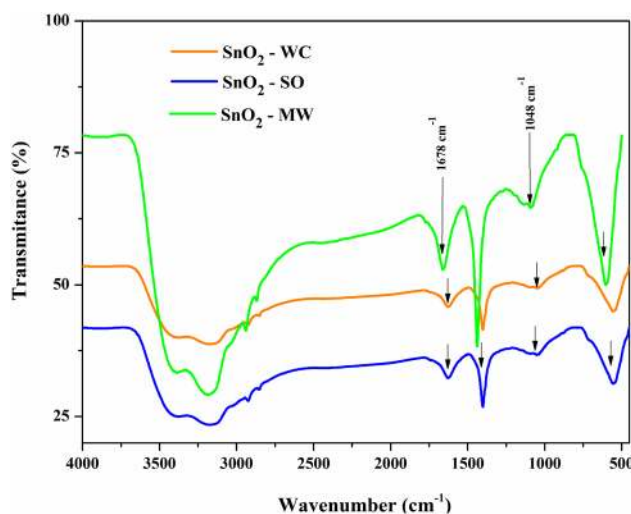


Fig. 12 shows FTIR Spectra of SnO₂ nanoparticles obtained after the degradation process

behaviour compared with the other two method influenced SnO₂ nanoparticles. It shows 90.8% of degradation efficiency in lesser than 150 min of UV light irradiation while 80%, 83.2% of degradation efficiency given by SnO₂-WC and SnO₂-SO nanoparticles. From the above brief experimental assessments, a green synthesized SnO₂ nanoparticle by microwave-assisted method is a potential candidate for pollutant dye degradation applications. In addition, this comparative assessment also helps to understand the influence of the processing method on the green synthesized SnO₂ nanoparticles which in turn helps in the tuning of nanoparticles as per the multifunctional applications.

Table 4 the comparative assessment of photocatalytic activity of prepared SnO₂ nanoparticles with existing reports

Name of the source	Part of the source	Photocatalyst	Dye	Dye concentration (g)	Reaction time (mins)	Degradation efficiency (%)	References
<i>Delonix elata</i>	Leaf	SnO ₂ -MW	Rhodamine B	0.2	150	92.47	This work
		SnO ₂ -SO	Rhodamine B	0.2	150	85.61	
		SnO ₂ -WC	Rhodamine B	0.2	180	81.30	
<i>C.betacea</i>	Fruit	SnO ₂	Methylene blue	0.5	70	85.1	[42]
<i>Calotropis gigantea</i>	Leaf	SnO ₂	Methyl orange	0.2	180	80.4	[43]
<i>Psidium Guajava</i>	Leaf	SnO ₂	RY186 dye	0.3	180	88.9	[44]
<i>cauliflower</i>	Leaf	SnO ₂	Methylene blue	0.2	180	88.2	[45]
			Rose Bengal	0.2	180	85	
<i>sugar cane</i>	sugar cane	SnO ₂	Methylene blue	0.2	180	87.9	[46]
			Rose Bengal	0.2	180	85	
<i>Bacteria</i>	<i>Erwinia herbicola</i>	SnO ₂	Methylene blue	0.2	160	93	[47]
			Methylene orange	0.2	160	93	

Compliance with ethical standards

Conflict of interest The authors declare that they have no conflict of interest.

References

- Khehra MS, Saini HS, Sharma DK, Chadha BS, Chimni SS (2005) Comparative studies on potential of consortium and constituent pure bacterial isolates to decolorize azo dyes. *Water Res* 39(20):5135–5141
- Junjie H (2015) Biosynthesis of SnO₂ nanoparticles by Fig *Ficus carica* leaf extract for electrochemically determining Hg (II) in Water samples. *Int J Electrochem Sci* 10:10668–10676
- Shah A, Lutfullah G, Ahmad K, Khalil AT, Maaza M (2018) *Daphne mucronata*-mediated phytosynthesis of silver nanoparticles and their novel biological applications, compatibility and toxicity studies. *Green Chem Lett Rev* 11(3):318–333
- Kavitha V, Mahalingam P, Jeyanthinath M, Sethupathi N (2020) Optical and structural properties of tungsten-doped barium strontium titanate. *Mater Today-Proc* 23(1):12–15
- Kasinathan MMK, Kennedy J, Elayaperumal M, Henini M (2016) Photodegradation of organic pollutants RhB dye using UV simulated sunlight on ceria based TiO₂ nanomaterials for antibacterial applications. *Sci Rep* 6(38064):1–12
- Fuku X, Diallo A, Maaza M (2016) Nanoscaled electrocatalytic optically modulated ZnO nanoparticles through green process of *Punica granatum* L. and their antibacterial activities. *Int J Electrochem* 2016:4682967. <https://doi.org/10.1155/2016/4682967>
- Kandasamy K, Surendhiran S, Syed Khadar YA, Rajasingh P (2020) Ultrasound-assisted microwave synthesis of CdS/MWCNTs QDs: a material for photocatalytic and corrosion inhibition activity. *Mater Today-Proc*. <https://doi.org/10.1016/j.matpr.2020.07.080>
- Is F, Imam S, Oki M, Ruey-an D (2020) One-pot biosynthesis of SnO₂ quantum dots mediated by *Clitoria ternatea* flower extract for photocatalytic degradation of rhodamine B. *J Environ Chem Eng* 8(4):103879
- Hassan D, Khalil AT, Saleem J, Diallo A, Khamlich S, Shinwari ZK, Maaza M (2018) Biosynthesis of pure hematite phase magnetic iron oxide nanoparticles using floral extracts of *Callistemon viminalis* (bottlebrush): their physical properties. *Artif Cell Nanomed B* 46(1):693–707
- Funda AA, Cebraïl G, Ali O, Ashraf HF, Guvenc A, Yuksel U, Zhi L (2013) Structural and electronic properties of SnO₂. *J Alloys Compd* 579:50–56
- Madubuonu N, Aisida SO, Ahmad I, Botha S, Zhao T, Maaza M, Ezema FI (2020) Bio-inspired iron oxide nanoparticles using *Psidium guajava* aqueous extract for antibacterial activity. *Appl Phys A* 126(1):1–8
- Adil S, Nafees A, Saima S, Suhail S, Mohammad ZK (2019) Ag₂S-sensitized NiO–ZnO heterostructures with enhanced visible light photocatalytic activity and acetone sensing property. *ACS Omega* 4:12905–12918
- Khalil AT, Ovais M, Ullah I, Ali M, Jan SA, Shinwari ZK, Maaza M (2020) Bioinspired synthesis of pure massicot phase lead oxide nanoparticles and assessment of their biocompatibility cytotoxicity and in vitro biological properties. *Arab J Chem* 13(1):916–931
- Mayedwa N, Mongwaketsi N, Khamlich S, Kaviyarasu K, Matinise N, Maaza M (2018) Green synthesis of zinc tin oxide (ZnSnO₃) nanoparticles using *Aspalathus Linearis* natural extracts: structural, morphological, optical and electrochemistry study. *Appl Surf Sci* 446:250–257
- Magdalane CM, Kaviyarasu K, Priyadharsini GMA, Bashir AKH, Mayedwa N, Matinise N, Isaev AB, Al-Dhabi NA, Mariadhas ValanArasu M, Arokiyaraj S, Kennedy J, Maaza M (2019) Improved photocatalytic decomposition of aqueous Rhodamine-B by solar light illuminated hierarchical yttria nanosphere decorated ceria nanorods. *J Mater Res Techno*; 8(3):2898–2909
- Hui-Chi C, Chen-Sheng Y (2007) Hydrothermal synthesis of SnO₂ nanoparticles and their gas-sensing of alcohol. *J Phys Chem C* 111:7256–7259
- Guanglu S, Jihuai W, Miaoliang H, Jianming L, Zhang L, Yunfang H, Fan L (2012) Facile synthesis of mesoporous tin oxide spheres and their applications in dye-sensitized solar cells. *J Phys Chem C* 116:20140–20145
- Panimalar S, Uthrakumar R, TamilSelvi E, Gomathy P, Inmozhi C, Kaviyarasu K, Kennedy J (2020) Studies of MnO₂/g–C₃N₄ heterostructure efficient of visible light photocatalyst for pollutants degradation by sol–gel technique. *Surf Interfaces* 20:100512
- Kaviyarasu K, Magdalane CM, Anand K, Manikandan E, Maaza M (2015) Synthesis and characterization studies of MgO: CuO nanocrystals by wet-chemical method. *Spectrochim Acta Part A Mol Biomol Spectrosc* 142:405–409
- Marikkannan M, Vishnukanthan V, Vijayshankar A, Mayandi J, Pearce JM (2015) A novel synthesis of tin oxide thin films by the sol–gel process for optoelectronic applications. *AIP Adv* 5:027122
- Elzbieta D, Grzegorz G, Joanna D, Andrzej B, Andrzej K, Magdalena PW (2017) Structural, chemical and optical properties of SnO₂ NPs obtained by three different synthesis routes. *J Phys Chem Solids* 107:100–107
- Arularasu MV, Anbarasu M, Poovaragan S, Sundaram R, Kanimozhi K, Maaza M (2018) Structural, optical, morphological and microbial studies on SnO₂ nanoparticles prepared by coprecipitation method. *J Nanosci Nanotechnol* 18(5):3511–3517
- Sudha M, Syed Khadar YA, Surendhiran S, Manojkumar P, Suresh KC, Balamurugan A (2020) Influence of synthesis methods on various properties of zinc oxide nanostructures. *Int J Anal Exp Model Anal* 12(1):1326–1338
- Suresh KC, Sudha M, Balamurugan A, Surendhiran S, Manojkumar P, Syed Khadar YA (2019) ZnO nanoparticles: biosynthesis and characterization of its multifunctional property. *J Inf Comput Sci* 9(12):401–413
- Sudha M, Balamurugan A, Surendhiran S, Manojkumar P, Syed Khadar YA (2019) Synthesis and characterisation of lanthanum added ZnO nanostructures. *J Inf Comput Sci* 9(12):396–406
- Govindarajan M, Sivakumar R, Rajeswari M, Yogalakshmi K (2012) Larvicidal and ovicidal properties of leaf and seed extracts of *Delonix elata* (L.) Gamble (Family: Fabaceae) against malaria (*Anopheles stephensi* Liston) and dengue (*Aedes aegypti* Linn.) (Diptera: Culicidae) vector mosquitoes. *Parasitol Res* 111:65–77
- Senthilkumar M, Sami Veerappa N (2014) Development and validation of GC–MS methods for determination of leaf and root of *Delonix elata* (L.) gamble. *Int J Adv Res Biol Sci* 1(2):93–107
- Sudha M, Surendhiran S, Manoj Kumar P, Balamurugan A (2020) Sonochemical synthesis of nickel doped ZnO nanostructures for environmental remediation. *Res Rev Int J Multidiscip* 05:11–16. <https://doi.org/10.5281/zenodo.3832132>
- Suresh KC, Balamurugan A (2020) Evaluation of structural, optical, and morphological properties of nickel oxide nanoparticles for multi-functional applications. *Inorg Nano-Met Chem*. <https://doi.org/10.1080/24701556.2020.1770793>

30. Balamurugan A, Sudha M, Surendhiran S, Devabharathi V, Syed Khadar YA (2020) Effect of calcination process on structural and optical properties of tungsten doped ZnO nanostructures. *RRIJM* 05:21–26. <https://doi.org/10.5281/zenodo.3837787>
31. Sathiya CK, Akilandeswari S (2014) Fabrication and characterization of silver nanoparticles using Delonix elata leaf broth. *SPECTROCHIM ACTA A* 128:337–341
32. De Mello VJ, Maia JRS, de Oliveira TT, Nagern TJ, Ardisson JD, De OPS, de Lima GM (2004) Tin (IV) compounds derivatives of reaction between Organotin (IV), SnCl_4 and rutin trihydrate: characterization and hypolipidemic effects. *Main Group Met Chem* 27:6. <https://doi.org/10.1515/MGMC.2004.27.6.309>
33. Tazikeh S, Akbari A, Talebi A, Talebi E (2014) Synthesis and characterization of tin oxide nanoparticles via the Co-precipitation method. *Mat Sci Pol* 32:98–101. <https://doi.org/10.2478/s13536-013-0164-y>
34. Elango G, Roopan SM (2016) Efficacy of SnO_2 nanoparticles toward photocatalytic degradation of methylene blue dye. *J Photochem Photobiol B Biol* 155:34–38. <https://doi.org/10.1016/j.jphotobiol.2015.12.010>
35. Kavitha V, Jeyanthinath M, Mahalingam P, Sethupathi N (2019) Structural, optical and electrical studies on zinc doped barium strontium titanate as photo-anode for DSSC device. *Mater Today-Proc.* <https://doi.org/10.1016/j.matpr.2019.05.437>
36. Khalil AT, Ovais M, Ullah I, Ali M, Shinwari ZK, Khamlich S, Maaza M (2017) *Sageretia thea* (Osbeck.) mediated synthesis of zinc oxide nanoparticles and its biological applications. *Nanomed* 12(15):1767–1789
37. Siva P, Surendhiran S (2019) Electrochemical reduction of CO_2 on $\text{Ni}(\text{OH})_2$ doped water dispersible graphene under different electrolyte conditions. *SN Appl Sci* 1:837. <https://doi.org/10.1007/s42452-019-0846-0>
38. Khalil AT, Ovais M, Ullah I, Ali M, Shinwari ZK, Hassan D, Maaza M (2018) *Sageretia thea* (Osbeck.) modulated biosynthesis of NiO nanoparticles and their in vitro pharmacognostic, antioxidant and cytotoxic potential. *Artif Cell Nanomed B* 46(4):838–852
39. Vasudevan D, Senthilkumar D, Surendhiran S (2020) Performance and characterization studies of reduced graphene oxides aqua nanofluids for a pool boiling surface. *Int J Thermophys* 41:74. <https://doi.org/10.1007/s10765-020-02651-6>
40. Khalil AT, Ovais M, Ullah I, Ali M, Shinwari ZK, Maaza M (2020) Physical properties, biological applications and biocompatibility studies on biosynthesized single phase cobalt oxide (Co_3O_4) nanoparticles via *Sageretia thea* (Osbeck.). *Arab J Chem* 13(1):606–619
41. Moones H, Morteza G, Atena N (2019) Biosynthesis of tin oxide (SnO_2) nanoparticles using jujube fruit for photocatalytic degradation of organic dyes. *Adv Powder Technol* 30:1551–1557
42. Ganesh E, Selvaraj MR (2015) Efficacy of SnO_2 nanoparticles towards photocatalytic degradation of methylene blue dye. *J Photochem Photobiol B Biol* 155:34–38. <https://doi.org/10.1016/j.jphotobiol.2015.12.010>
43. Bhosale TT, Shinde HM, Gavade NL, Babar SB, Gawade VV, Sabale SR, Kamble RJ, Shirke BS, Garadkar KM (2018) Biosynthesis of SnO_2 nanoparticles by aqueous leaf extract of *Calotropis gigantea* for photocatalytic applications. *J Mater* 29:6826–6834
44. Mandeep K, Akansha M, Amit M, Jagpreet S, Mohit R, Soumen B (2017) Biosynthesis of tin oxide nanoparticles using *Psidium guajava* leave extract for photocatalytic dye degradation under sunlight. *Mater Lett* 215:121–124. <https://doi.org/10.1016/j.matlet.2017.12.074>
45. Jejenija O, Damian CO, Eno EE (2017) Biosynthesis and photocatalytic properties of SnO_2 nanoparticles prepared using aqueous extract of cauliflower. *J Clust Sci* 28:1883–1896
46. Archita B, Ahmaruzzaman M (2015) Photocatalytic-degradation and reduction of organic compounds using SnO_2 quantum dots (via green route) under direct sunlight. *RSC Adv* 5:66122–66133. <https://doi.org/10.1039/C5RA07578E>
47. Srivastava N, Mukhopadhyay M (2014) Biosynthesis of SnO_2 nanoparticles using bacterium *Erwinia herbicola* and their photocatalytic activity for degradation of dyes. *Ind Eng Chem Res* 53:13971–13979. <https://doi.org/10.1021/ie5020052>

Publisher's Note Springer Nature remains neutral with regard to jurisdictional claims in published maps and institutional affiliations.